J. Micromech. Microeng. **19** (2009) 015025 (9pp) doi:10.1088/0960-1317/19/1/015025

Liquid transfer between two separating plates for micro-gravure-offset printing

Hyun Wook Kang[1], Hyung Jin Sung[1], Taik-Min Lee[2], Dong-Soo Kim[2] and Chang-Jin Kim[3]

[1] Department of Mechanical Engineering, KAIST, 373-1 Guseong-dong, Yuseong-gu, Daejeon 305-701, Korea
[2] Nano Convergence Machinery Research Division, 171 Jang-dong, Yuseong-gu, Daejeon 305-343, Korea
[3] Mechanical and Aerospace Engineering Department, University of California at Los Angeles, Los Angeles, CA 90095-1597, USA

E-mail: hjsung@kaist.ac.kr

Received 31 August 2008, in final form 1 November 2008
Published 10 December 2008
Online at stacks.iop.org/JMM/19/015025

Abstract
Experimental investigations of the liquid transfer between two separating plates have been carried out, with the aim of increasing the ink transfer ratio in micro-gravure-offset printing. A sessile droplet is divided into two by moving one plate vertically with respect to a fixed plate. The surface contact angles of the sessile droplet on the two plates were of particular interest in this study because the volume ratio of the two droplets varies with the contact angles. Various methods for controlling the surface contact angle, including chemical treatment, plasma surface modification and electrowetting-on-dielectric were assessed. Image analysis of the droplets was carried out to estimate the surface contact angles and to measure the volumes of the droplets. The liquid transfer process and related phenomena, such as satellite droplet generation and the variation in the contact areas between the droplets and the plates, were observed. The experimental results help us to determine the optimal surface contact angles of the plate cylinder, blanket cylinder and substrate for micro-gravure-offset printing.

1. Introduction

Printing technologies have long been used in the graphics industry to produce printed media. The processes can be classified according to the printing method, such as jet printing [1], gravure-offset printing [2], screen printing [3] and flexographic printing. New printing technologies have recently gained increased attention because of their superior price competitiveness over the existing lithographic processes in manufacturing a wide range of devices including displays, electronic paper and RFID (radio frequency identification) tags. The lithographic processes that are widely used for semiconductors and MEMS (micro-electro-mechanical systems) require long manufacturing times and expensive equipment, and waste considerable quantities of materials by etching them with harsh chemicals. As a result, in spite of their poor resolution, printing technologies are considered favorably for the above new devices because of rapid processes, mass production ability, low cost both in equipment and production and so on.

Of the several available printing processes, the micro-gravure-offset printing technique, which was traditionally been used in the graphic printing industry to produce items such as magazine covers and newspaper supplements [4], has recently received much attention as a potential method for the cost-effective mass-production of micro-scale electrical circuits [2]. Since the offset printing process is a direct contact patterning method and can be used with roll-to-roll web feeding systems, it has the advantage of higher productivity than other printing processes. In micro-gravure-offset printing, schematically described in figure 1, ink from an ink reservoir is first poured into the grooves of a gravure plate cylinder or roller, and the excess ink is removed with a doctor blade. The ink in the grooves is then picked up with a silicone rubber blanket cylinder. Finally, the cylinder is rotated over the target substrate, thereby transferring the ink onto the substrate. Ultraviolet (UV) or thermal drying is

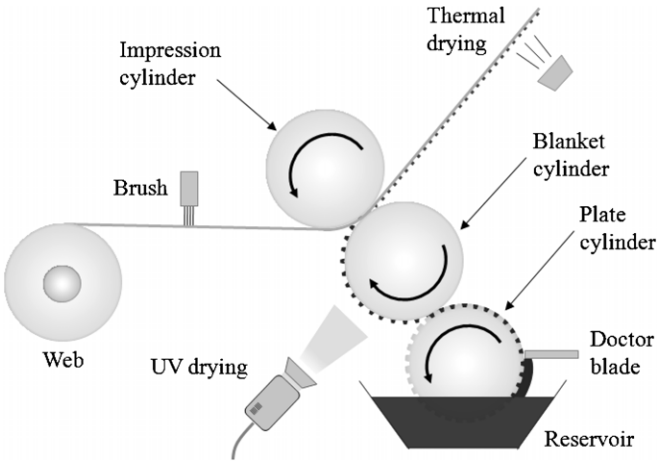

Figure 1. Schematic of a typical micro-gravure-offset printing process.

used to control the properties of the ink and cylinder surfaces during the printing process. The brush cleans the substrate before contact with the blanket cylinder and thus maintains its stability and uniformity.

Various experimental studies have demonstrated the printing of narrow conductor lines with widths on the order of micrometers with gravure-offset printing. Mikami *et al* [5] proposed a gravure-offset printing method for the patterning of large area thin film transistors without the use of an optical mask aligner. Lahti *et al* [6] discussed the various aspects of gravure-offset printing affecting the fabrication of thick films, such as the printing plate, the silicone rubber pad and the printing ink. Hagberg *et al* [7] presented a new method to manufacture plates for the gravure printing of fine line thick film circuits. They investigated the relationships between various aspects of gravure-offset printing, in particular between pattern geometries and printing inks. The ink-transfer efficiency and print quality are affected by many factors. Elsayad *et al* [8] discussed the factors affecting ink transfer and concluded that printing speed, printing pressure, ink viscosity and the type of ink resin influence the transfer of the ink to the paper. Pudas *et al* [9] examined the aspects of gravure-offset printing and ink components affecting its use in electronics applications. These studies concluded that both material surface and ink factors affect the ink transfer process in micro-gravure-offset printing.

Some numerical studies of the factors affecting ink transfer and related problems in micro-gravure-offset printing processes have been performed. Darhuber *et al* [10] carried out numerical simulations with the Surface Evolver software [11], which takes into account the liquid's surface tension and the liquid–solid interfacial energy. Steepest descent and conjugate gradient methods were implemented in the minimization of total energy. Two numerical examples were presented: the equilibrium shape of the ink meniscus between two parallel plates, and the equilibrium shape of the ink meniscus between the stamp and the target substrate for a small tilt of 2°. Their simulations assumed quasistatic printing and unconstrained contact line motion, so the results were only affected by the surface contact angle, regardless of the properties of the ink. Zhang [12] carried out numerical simulations of drop formation using the VOF (volume of fluid) method that were in good agreement with experimental results. In their simulations, they studied the breakup of the liquid filament and the subsequent generation of satellite droplets. Huang *et al* [13] proposed and implemented a numerical model for simulating liquid transfer during the micro-gravure-offset printing process. In particular, the printing of ink from the offset pad onto the substrate was modeled in terms of the liquid transfer between two parallel separating plates, and the picking up of ink from the gravure plate by the offset pad was modeled in terms of the liquid transfer between a trapezoidal cavity and an upward moving plate.

In the gravure-offset printing technique used in the media printing industry, printing failures, such as a missing dot or a line break, are not significant. However, in the micro-gravure-offset printing used to produce electrical devices and display components, such printing failures have to be eliminated and the line width should be in micrometers. For these requirements, the volume of printed ink needs to be estimated, which prompted us to investigate the liquid transfer rate with the aim of enhancing the micro-gravure-offset printing performance. In the present study, we investigated the liquid transfer process experimentally, in particular the effects of surface contact angles on the two opposing plates. The desired contact angles were obtained by modifying the surface properties with chemical treatment, plasma surface modification and electrowetting-on-dielectric (EWOD) [14]. The liquid transfer ratio was measured by analyzing images of the droplets. The droplet volumes and surface contact angles were determined by analyzing the droplet geometries.

2. Experimental setup

In the micro-gravure-offset printing process, the ink transfer occurs between two rotating cylinders, so the dynamic effects created by the rotational motion of the cylinders have to be considered. In a typical system, the diameters of the cylinders are on the order of 10^5 μm, and the pattern on the plate cylinder or the printed width is on the order of 10–10^2 μm [15]. The difference between these sizes means that the dynamic effects caused by the rotational motion of the cylinders during the ink transfer process can be neglected, so that the ink transfer in micro-gravure-offset printing can be regarded as that between two parallel plates. In the present study, our experimental approach to the estimation of the liquid transfer rate used two plates placed in parallel, one of which could be moved vertically toward and away from the other plate.

Figure 2(*a*) shows the starting point for the experiment on each droplet. Films processed with various surface treatments were attached to the upper and lower plates to provide various surface contact angles, which can be used as a measure of the adhesion between the solid and the liquid and to characterize the surfaces in the micro-gravure-offset printing process. In the present study, the contact angles were varied with several methods: altering the liquid properties and altering the surface properties with surface treatments, e.g., Teflon coating, PMMA (polymethylmethacrylate) coating, plasma treatment

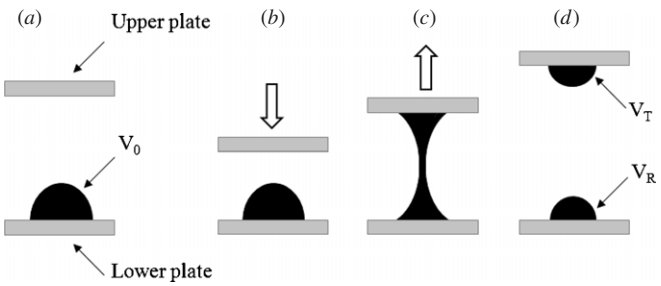

Figure 2. The droplet separation process.

Table 1. Parameters of the liquid transfer between two parallel plates.

Upper plate velocity, U	2.8 mm s^{-1}
Lower plate velocity	0 m s^{-1}
Electrical conductivity of the liquid	5.5×10^{-6} S m^{-1}
Density of the liquid, ρ	997 kg m^{-3}
Dynamic viscosity of the liquid, μ	1.003×10^{-3} N s m^{-2}
Surface tension coefficient, σ	
PET	42.1 dynes cm^{-1}
PMMA	41.1 dynes cm^{-1}
Teflon	23.9 dynes cm^{-1}
Acceleration due to gravity, g	9.81 m s^{-1}
Volume of the liquid droplet, V	4 μl
Minimum distance between the two plates, d	0.25 mm

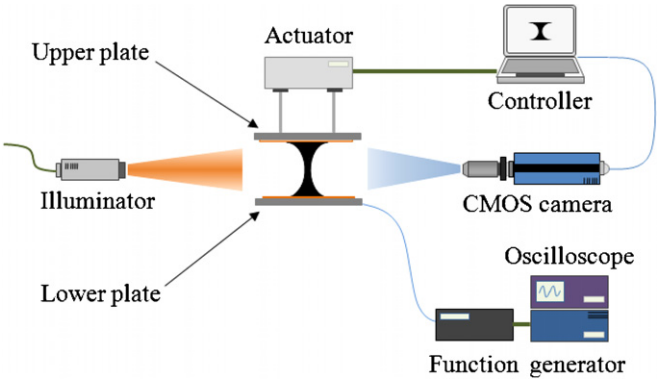

Figure 3. Experimental setup.
(This figure is in colour only in the electronic version)

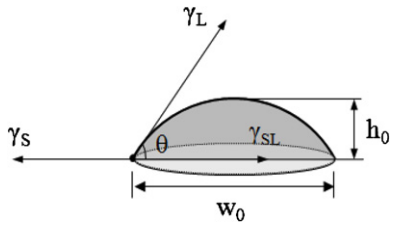

Figure 4. Geometry of the droplet cross section; point shape droplet (axisymmetric).

and electric control by EWOD. These processes are discussed in the following section. The experiments were carried out with the following method. After the films are attached to the plates, a 4 μl droplet of pure water is placed on the lower plate with a micropipette, and then the upper plate is moved down toward the lower plate with a uniform velocity. As the upper plate moves closer to the lower plate, the droplet bridges the two plates, contacting the two films. As the upper plate moves vertically away, the droplet is divided into two droplets, one each on the upper and lower plates. A schematic diagram of the liquid transfer process is shown in figure 2. The experimental parameters are listed in table 1.

Figure 3 shows a schematic diagram of the experimental setup. Movement of the upper plate is controlled with an air pressure actuator at 2.8 mm s^{-1}. The lower plate is fixed during the experiment to maintain droplet stability before the droplet makes contact with the upper plate. The illuminator creates a brightness difference between the liquid and gas regions, which makes the droplet boundary much clearer. The initial droplet and the droplet division process were captured with a CMOS (complementary metal-oxide semiconductor) camera. The captured images were analyzed to measure the surface contact angles and to observe the liquid transfer process. Additionally, a voltage amplifier and a function generator were used to test EWOD films.

3. Results and discussion

3.1. Surface contact angle

The surface contact angle that arises when a liquid is placed on a solid surface can be analyzed in terms of thermodynamic equilibrium. Since three phases are present—liquid, solid and gas/vapor—their chemical potentials should be equivalent at their contact points. The three interfacial energies are γ_S (surface tension of the solid), γ_L (surface tension of the liquid) and γ_{SL} (interfacial tension between the solid and the liquid); the surface tension is equal to the surface free energy per unit area. The equation describing this equilibrium can be written as

$$\gamma_L \cos\theta = \gamma_S - \gamma_{SL}, \tag{1}$$

which is known as Young's equation [16]. The geometrical relationships are shown in figure 4, where θ denotes the contact angle of the liquid. The relationship describing the adhesion work between the solid and the liquid can be expressed as [17]

$$\Delta G_{SL} = \gamma_{SL} - \gamma_S - \gamma_L, \tag{2}$$

where ΔG_{SL} is the free energy of adhesion. Combining equations (1) and (2), we obtain the Young–Dupré equation:

$$-\Delta G_{SL} = \gamma_L(1 + \cos\theta). \tag{3}$$

In general, $-\Delta G_{SL}$ has a positive value, so the free energy of adhesion increases as θ decreases for $0 \leqslant \theta \leqslant \pi$. The interfacial force between the solid and the liquid can be estimated from the measured contact angle of a droplet by using this physical relation [18].

3.2. Droplet geometry

Printed ink or liquid can be modeled with various shapes including a point, which is axisymmetric as shown in figure 4. In this study, the droplets were assumed to be truncated spheres, i.e., the cross-sections are partial circles,

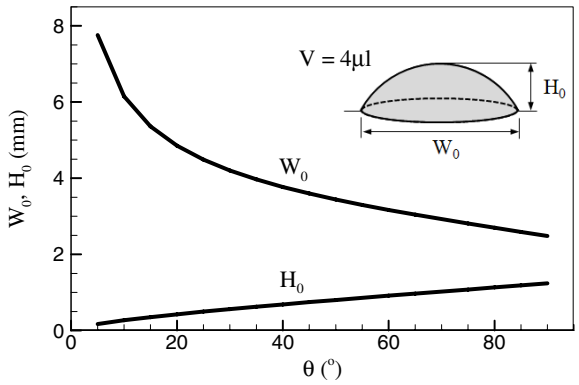

Figure 5. Variations of the width and height of the liquid droplet with the contact angle.

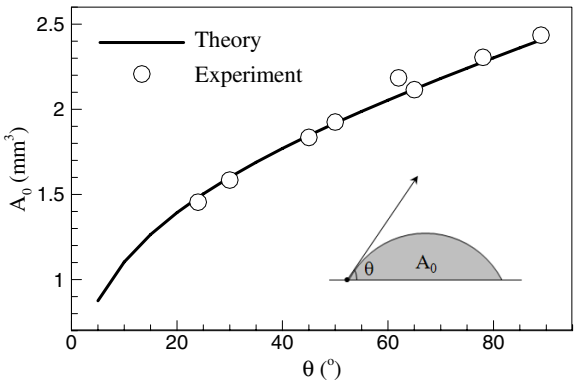

Figure 6. Area of the liquid droplet cross section with the contact angle.

as shown in figure 4. By obtaining a side view of each droplet by lining up an illuminator, the droplet and a camera (figure 3) and using image analysis, the contact angle and the geometrical parameters indicated in figure 4 were obtained for each droplet. The contact angle can be related to the geometrical parameters with equations (4) and (5). The contact angles are in radians in all the equations in this paper. With this relation, we can obtain the contact angles of the droplets from the captured images:

$$\theta(w_0, h_0) = \sin^{-1}\left[w_0 h_0 \big/ \left(h_0^2 + w_0^2/4\right)\right], \quad h_0 \leqslant w_0/2, \tag{4}$$

$$\theta(w_0, h_0) = \cos^{-1}\left[w_0 h_0 \big/ \left(h_0^2 + w_0^2/4\right)\right] + \pi/2, \quad h_0 \geqslant w_0/2, \tag{5}$$

where w_0 and h_0 denote the contact diameter and the height of the droplet, respectively, derived from the captured geometric image as the width and height of the droplet cross-section. The two values of w_0 and h_0 are also expressed with the contact angle for a given liquid volume V using equations (6) and (7):

$$w_0 = 2\sin\theta[3V(\sin^2\theta\cos\theta + 2\cos\theta + 2)/\pi]^{1/3}, \tag{6}$$

$$h_0 = (1 - \cos\theta)[3V(\sin^2\theta\ \cos\theta + 2\cos\theta + 2)/\pi]^{1/3}. \tag{7}$$

The volume of water droplets used in the experiments is 4 μl. Each droplet image was analyzed in units of pixels. Figure 5 shows the variations with the contact angle of the width and height of the cross-section of a 4 μl droplet, which enables the facile determination of the contact angles of the droplets.

As discussed above, the width and height of the cross-section of each droplet were estimated by counting the pixels in the appropriate directions. The shift to the right or left is not significant because the captured area of droplet side view does not change. However, if the shift is fore or back to the camera, the captured area will be changed, causing an error in the measurement of the transfer ratio. Since the droplet image may be shifted from the true droplet cross-section in our experiment, causing erroneous results, the values were validated by calculating the area of the droplet cross-section from the captured image. The area of the droplet cross-section (A_0) can be expressed as

$$A_0 = (\theta - \sin\theta\cos\theta)[3V(\sin^2\theta\cos\theta + 2\cos\theta + 2)/\pi]^{2/3}. \tag{8}$$

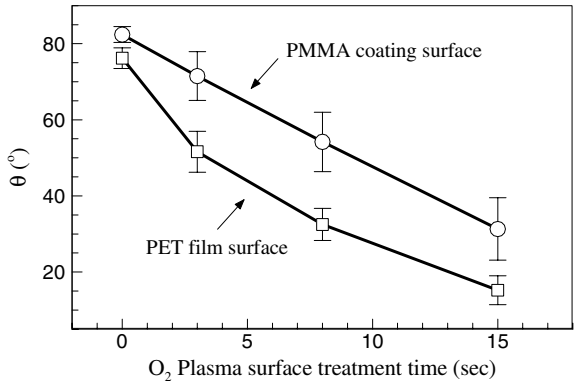

Figure 7. Contact angle depending on the O_2 plasma surface treatment time.

Figure 6 shows the values of A_0 as a function of θ obtained in the present experiments as well as the theoretical solutions, i.e. of equation (8). The experimental results are in good agreement with the theoretical curves.

3.3. Surface treatment

The purpose of this study was to measure the dependence of the transfer ratio on the surface contact angles. Various methods were employed to prepare the surfaces with different contact angles. First, we consider plasma surface modification. Plasma processing is used in numerous industry applications, e.g., the enhancement of paint adhesion, the improvement of bonding in polymer matrix composites and the cleaning of material surfaces [19]. Plasma processing tends to make surfaces more hydrophobic or hydrophilic. The main roles of plasma processing are surface cleaning and the modification of the surface chemical structure. In these processes, the plasma processing modifies the physical and chemical properties of the surface. Adhesion is governed by a surface layer of molecular dimensions. Hence, with plasma processing the surface adhesion, wettability and printability of a material surface can be controlled. Figure 7 shows the variation in the contact angles on the PET (polyethylene terephthalate) film and PMMA (polymethylmethacrylate) coating surface with the O_2 plasma surface treatment time at a pressure of 200 mTorr and a power of 50 W. The wetting characteristics

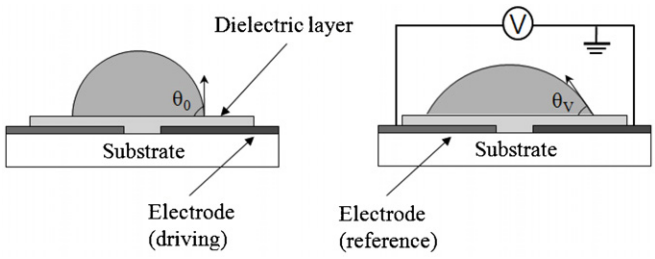

Figure 8. Contact angle changes by electrical potential on the electrowetting surface; electrowetting-on-dielectric of single-side coplanar electrodes.

of the surfaces change over time and are represented by the surface contact angles. To avoid the influence of such changes, we performed our experiments within 1 min after the surface treatment process. Among our tested samples, the plasma-treated surface was most challenging, mostly affected by surrounding conditions and printing fluid. To assure a uniform surface condition during printing, the intensity of plasma had to be well controlled during the surface treatment.

Surface coating is another method for surface treatment and includes many processes such as various chemical vapor depositions, evaporation, sputtering and spin coating. In our study, we obtained contact angles on the PET film of $\theta = 72.8^\circ \pm 4.4^\circ$ in the absence of any coating, $\theta = 82.4^\circ \pm 4.2^\circ$ by adding a PMMA coating and $\theta = 112.9^\circ \pm 1.8^\circ$ by adding a Teflon coating. Electrowetting enables the active control of surface wettability by changing the surface free energy through the application of an electric potential. Typically, the voltage is applied between a liquid and the underneath electrode, which is covered with a dielectric layer (thus EWOD). More specifically in this study, a coplanar electrode design [20] was used, as illustrated in figure 8, which keeps the top of the droplet free for liquid transfer. When a voltage is applied, the contact angle of the liquid is decreased (bottom figure) from its initial value (top figure). The contact angles on different surface materials are visualized in figure 9 (Teflon coating surface; $t_d \simeq 3.5$ μm, PMMA coating surface; $t_d \simeq 3.2$ μm). The relationship between the applied voltage and the contact angle can be formulated by combining Lipmann's and Young's equations as

$$\cos\theta_V - \cos\theta_0 = \frac{\varepsilon_r \varepsilon_0}{2\gamma_L t_d} V^2, \qquad (9)$$

where θ_V and θ_0 are the contact angles for the applied voltages V and 0, respectively, ε_r and ε_0 are the dielectric constant of the insulating layer and the permittivity of vacuum, respectively, and t_d is the thickness of the dielectric layer [14].

To note that liquid properties affect the contact angle as well, we tested the effect of a surfactant added to the water droplets. Figure 10 shows the dependence of the surface contact angle on the surfactant ratio. The repeatability of the surface contact angles has been presented as error bars. One error range was obtained from measurements of more than 10 times. Since the volume of added surfactant is very small, the change in viscosity of the water droplet is negligible.

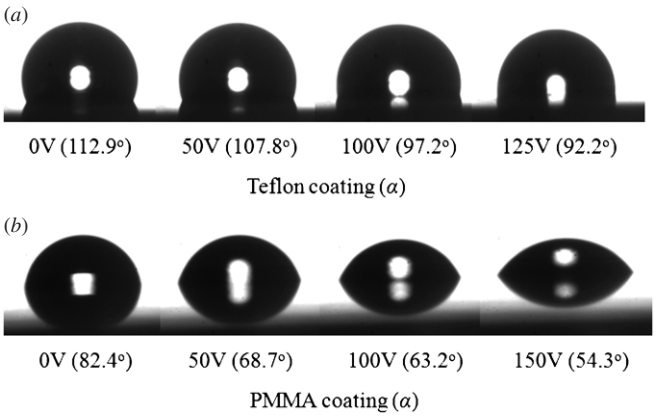

Figure 9. Pictures of sessile drop on the electrowetting-on-dielectric depending on the applied voltage: (*a*) Teflon coating surface and (*b*) PMMA coating surface.

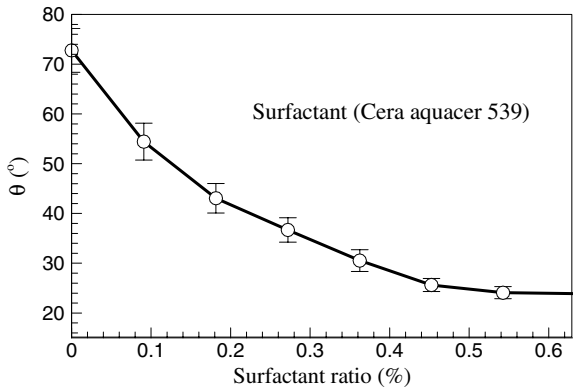

Figure 10. Contact angle depending on the surfactant ratio.

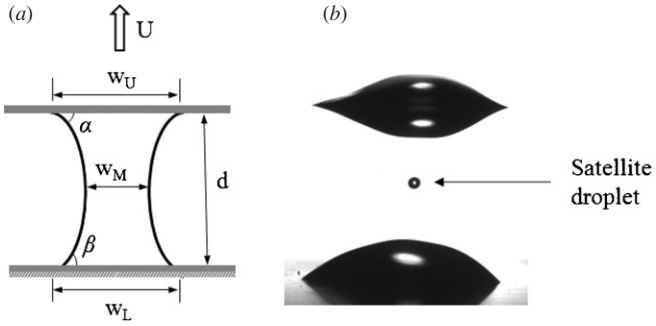

Figure 11. (*a*) Droplet filament between the upper plate and the lower plate and (*b*) captured image of a satellite droplet.

3.4. Transfer ratio

The transfer ratio for the division of the droplets between two separating plates was measured by analyzing the droplet images, which consist of a shadow region (the droplet side view) and a bright region (the ambient gas). Figure 11(*a*) shows a schematic diagram of the cross-section of a droplet filament, α and β are the contact angles on the upper and lower plates, respectively, U is the operation velocity of the upper plate, d is the distance between the upper and lower plates and w_U and w_L are the contact widths at the upper and lower

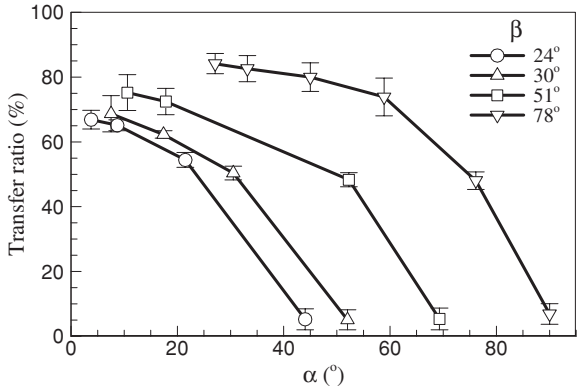

Figure 12. Variation of the transfer ratio with the surface contact angle.

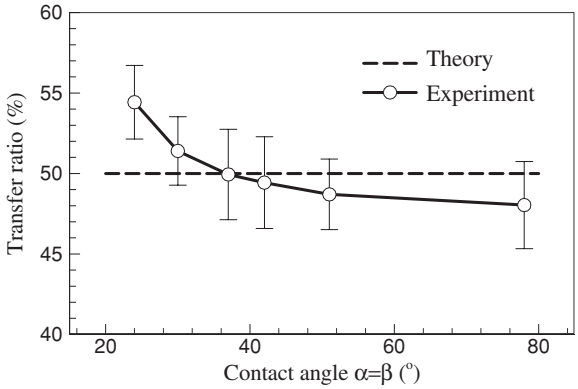

Figure 13. Transfer ratio for $\alpha = \beta$.

plates, respectively. w_M is the minimum diameter of the liquid filament during the transfer process.

From the captured image, we can obtain w_0 (the contact diameter of the droplet) and h_0 (the height of the droplet), as shown in figure 4. If the droplet is assumed to be a truncated sphere, the volume of the droplet is given by

$$V(w_0, h_0) = \pi h_0^2\left[\left(h_0^2 + w_0^2/4\right)/2h_0 - h_0/3\right]. \quad (10)$$

The transfer ratio is then given by

$$\mathrm{tr}\% = [V_t/V] \times 100\% = [(V - V_r)/V] \times 100\%, \quad (11)$$

where V is the initial volume, V_t is the transferred liquid volume and V_r is the remaining liquid volume (figure 2). The final liquid transfer ratio depends on the contact angles, as shown in figure 12. The upper plate moves at a speed of 2.8 mm s^{-1}, and it remains for 2 s in its lowest position. The liquid transfer was measured more than 10 times for each condition. The transfer ratio increases as the contact angle on the upper plate (α) decreases and the contact angle on the lower plate (β) increases. The transfer ratio is high for a small α but decreases rapidly as α increases toward and becomes greater than β in every case. When α and β are similar, the transfer ratio is close to 50%. These results show that the transfer ratio for the division of a droplet between two separating plates depends strongly on the contact angles of the droplet on the two plates. Since the contact angle is a measure of the surface free energy, the liquid transfer process can be understood as occurring due to the interaction between liquid and solid surface energy. Thus, the liquid transfer ratio can be controlled by altering the surface free energy or liquid characteristics. From this point of view, in order to increase the ink transfer ratio in the micro-gravure-offset printing process, the characteristics of the plate cylinder, the blanket cylinder, the substrate and the ink should be taken into consideration.

Under the quasistatic assumption, the final transfer ratio is independent of the separation velocity and the properties of the liquid, and can be derived theoretically:

$$\mathrm{tr}\% = f(a)/(f(a) + f(\beta)) \times 100\%, \quad (12)$$

where

$$f(x) = \begin{cases} -\pi/4 + x/2 + \cos x - \sin x\ \cos x/2, \\ \quad \text{symmetric} \\ -\pi/2 + x/2 + \cos x - \sin x\ \cos x - (\cos x)^3/3, \\ \quad \text{axisymmetric}, \end{cases}$$

$x = \alpha$ or β.

Here, $f(x)$ is a function of the liquid volume that can be obtained by assuming that the free surface has a circular shape [13]. According to equation (12), a liquid transfer ratio of 50% is obtained when $\alpha = \beta$; the experimental results are shown in figure 13. The experimental values of the liquid transfer ratio when $\alpha = \beta$ are close to 50%. However, the transfer ratio increases slightly as the contact angle decreases. The differences between the theoretical and experimental results increase as the contact angle decreases. We consider that the errors were caused by the effect of the dynamic surface free energy. The dynamic surface free energy increases as the surface contact angle decreases.

Note that shifts in the droplet positions produced when the two plates are not exactly parallel or by equipment vibration were taken into account in these experiments. A shift to the right or left is not significant because the area captured in the droplet side view does not change. However, if the shift is forward or backward with respect to the camera, the captured area changes, resulting in an error in the measurement of the transfer ratio. To address this issue, we measured the droplet shift during the measurements, leading to the error analysis shown in figure 14. The distance of the droplet shift was estimated to be in the range 0.2–1.1 mm. This error analysis indicates that the resulting errors in image processing are less than ±3%, and so do not significantly affect the results for the final transfer ratio.

3.5. Liquid transfer process

Figure 15 shows the variation during the experiment in the distance (d) between the two separating walls. Sequential images of the division of droplets between two parallel plates are displayed in figure 16. As the upper plate moves upward, the liquid droplet is stretched and a filament is created in the middle of the droplet. The droplet contact diameters

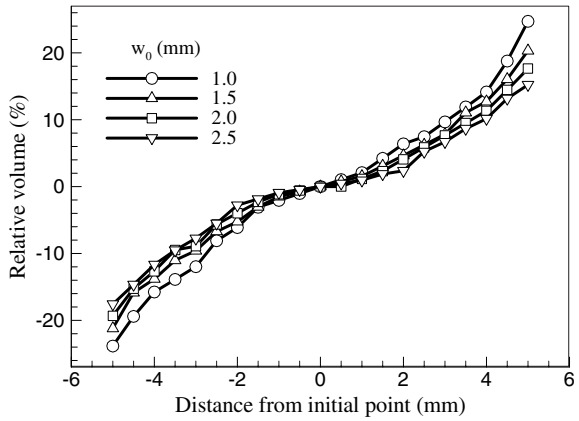

Figure 14. Analysis of the error due to variations in droplet position.

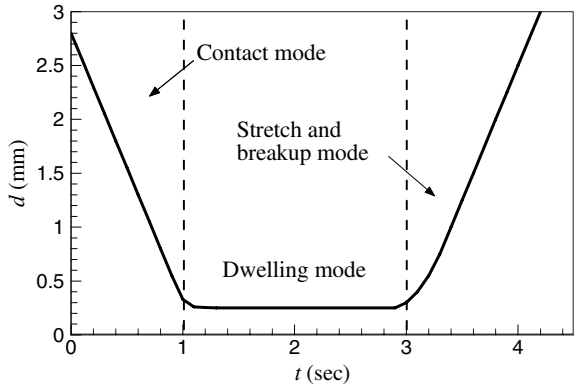

Figure 15. Distance (d) between two separating plates during experiment.

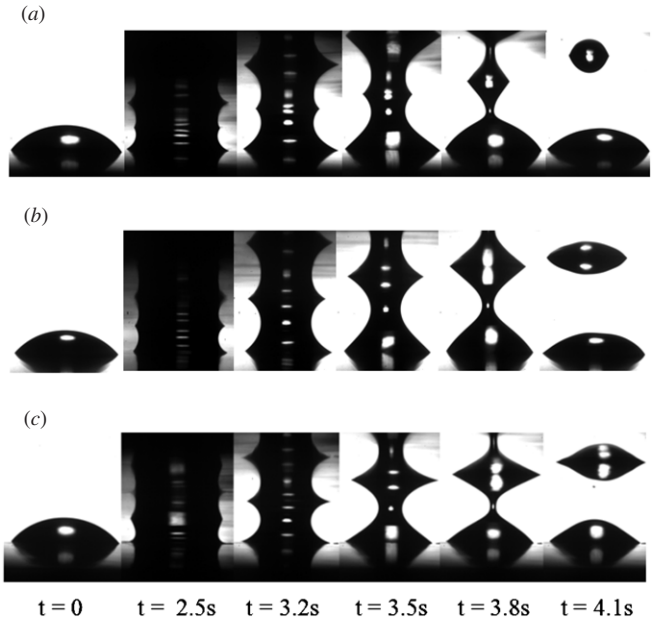

Figure 16. Sequential pictures of droplet separation between two parallel plates with $\beta = 45^\circ$ and (a) $\alpha = 78^\circ$, (b) $\alpha = 50^\circ$ and (c) $\alpha = 45^\circ$.

on the upper and lower plates change simultaneously due to the surface tension. After the filament is broken, the two droplets recoil toward the plates, then the liquid droplets on

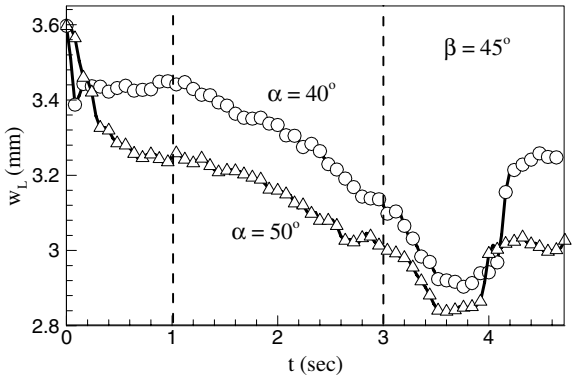

Figure 17. Time histories of the contact diameter of liquid on the lower plate (w_L).

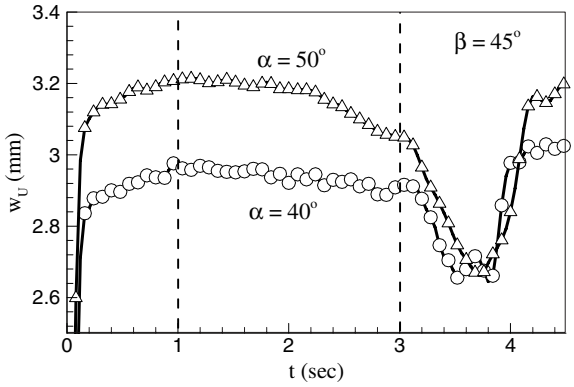

Figure 18. Time histories of the contact diameter of liquid on the upper plate (w_U).

both plates attain their equilibrium shapes, and division is complete. During the breakup process, a satellite droplet can be generated. The formation of this droplet is similar to the behavior observed during drop formation from a nozzle or orifice [12], which was found to be caused by the double breakage of the liquid filament [21]. Huang *et al* [13] have carried out a numerical analysis of satellite droplet generation during the liquid transfer process.

In the contact mode (figure 15), the upper plate moves down toward the droplet, and then makes contact with the droplet's apex. After the upper plate reaches its lowest position, it remains there in the dwelling mode for 2 s. During this dwelling mode, the liquid filament moves toward its equilibrium shape, which depends on the upper and lower plate surface contact angles; the shape of the liquid filament is shown schematically in figure 11. As the upper plate starts moving upward again, the liquid filament stretches and breaks up.

The time histories of the contact diameters of the liquid on the lower plate (w_L) and the upper plate (w_U) are shown in figures 17 and 18, respectively; the contact angle on the lower plate in these figures is $\beta = 45^\circ$ and on the upper plates are $\alpha = 40^\circ$ and 50°, respectively. As shown in figure 17, w_L decreases slightly during the dwelling mode, and this trend is maintained until the breakup of the liquid filament. w_L increases sharply due to the recoil of the liquid after the breakup. On the other

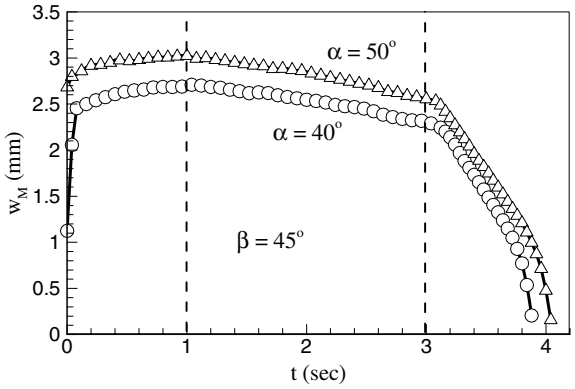

Figure 19. The minimum thickness of the liquid filament (w_M).

hand, w_U remains almost constant during the dwelling mode. At the beginning of the stretch and breakup mode, however, w_U decreases sharply and finally increases due to the recoil of the droplet, as in the case of w_L. The trends of the liquid transfer process resemble both w_U and w_L except the dwelling mode as shown in figures 17 and 18. The variation of the minimum thickness of the liquid filament (w_M) during the transfer process is shown in figure 19. These results were obtained for $\beta = 45°$, $\alpha = 40°$ and 50°. w_M is monitored from the moment the upper plate makes contact with the droplet. At the contact, the liquid filament forms instantaneously, then w_M decreases drastically during the stretch and breakup mode, and finally liquid breakup occurs.

4. Conclusion

We have carried out a study of the liquid transfer between two separating plates to investigate ink transfer in micro-gravure-offset printing. From the ink transfer experiments, the relation between the surface contact angle and surface free energy was examined. The relationship between the surface contact angle and the ink transfer ratio was investigated quantitatively. Chemical treatment, plasma surface modification and electrowetting-on-dielectric were used to obtain various surface contact angles. The degree of liquid transfer was calculated by analyzing droplet images. Our results show that the liquid transfer ratio increases as the contact angle of the droplet on the lower plate increases and as the contact angle on the upper plate decreases. The liquid droplet adheres more strongly to the plate with higher surface energy. Ink transfer takes place twice in micro-gravure-offset printing. Hence, the blanket cylinder located between the plate cylinder and the substrate should have the appropriate surface contact angle. A low surface contact angle will result in a decrease in the transfer ratio when the liquid is transferred from the blanket cylinder to the substrate, and a high surface contact angle will result in a decrease in the transfer ratio when ink is transferred from the plate cylinder to the blanket cylinder. The liquid transfer process was divided into three modes: (1) the contact mode; (2) the dwelling mode; (3) the stretch and breakup mode, depending on the position of the surface of the upper plate. During the liquid transfer process, the stretching, breaking and recoil of the liquid droplet were observed during the stretch and breakup mode. A liquid filament is formed when the upper plate makes contact with the liquid droplet. The minimum thickness of the filament decreases drastically during the stretch and breakup mode, and then finally liquid breakup occurs.

Acknowledgment

This work was supported by the Korea Foundation for International Cooperation of Science and Technology (KICOS) through the Global Partnership Program in K20602000002. The authors wish to thank Drs B J Kim and J Gong for helpful discussion and technical support.

References

[1] Lee T-M, Kang T G, Yang J S, Jo J, Kim K-Y, Choi B-O and Kim D-S 2008 Drop-on-demand solder droplet jetting system for fabricating micro structure *IEEE Trans. Electron. Packag. Manuf.* **31** 202–10
[2] Pudas M 2004 *Gravure-offset Printing in the Manufacture of Ultra-fine-line Thick-films for Electronics* (Oulu University Press)
[3] Lee T-M, Choi Y-J, Nam S-Y, You C-W, Na D-Y, Choi H-C, Shin D-Y, Kim K-Y and Jung K-I 2008 Color filter patterned by screen printing *Thin Solid Films* **516** 7875–80
[4] Odiotti M E and Colaprico V 1991 *Gravure process and technology* Gravure Association of America, Gravure Education Foundation
[5] Mikami Y *et al* 1994 A new patterning process concept for large-area transistor circuit fabrication without using an optical mask aligner *IEEE Trans. Electron. Dev.* **41** 306–14
[6] Lahti M, Leppävuori S and Lantto V 1999 Gravure-offset-printing technique for the fabrication of solid films *Appl. Surf. Sci.* **142** 367–70
[7] Hagberg J, Pudas M, Leppävuori S, Elsey K and Logan A 2001 Gravure offset printing development for fine line thick film circuits *Microelectron. Int.* **18** 32–5
[8] Elsayad S, Morsy F, El-Sherbiny S and Abdou E 2002 Some factors affecting ink transfer in gravure printing *Pigment Resin Technol.* **31** 234–40
[9] Pudas M, Hagberg J and Leppävuori S 2004 Printing parameters and ink components affecting ultra-fine-line gravure-offset printing for electronics applications *J. Eur. Ceram. Soc.* **24** 2943–50
[10] Darhuber A A, Miller S M, Troian S M and Wagner S 2000 Process simulation for contact print microlithography *Tech. Proc. 2000 Int. Conf. on Modeling and Simulation of Microsystems* chapter 2
[11] Brakke K A 1992 The surface evolver *Exp. Math.* **1** 141–65
[12] Zhang X 1999 Dynamics of drop formation in viscous flows *Chem. Eng. Sci.* **54** 1759–74
[13] Huang W-X, Lee S-H, Sung H J, Lee T-M and Kim D-S 2008 Simulation of liquid transfer between separating walls for modeling micro-gravure-offset printing *Int. J. Heat Fluid Flow* **29** 1436–46
[14] Moon H, Cho S K, Garrell R L and Kim C-J 2002 Low voltage electrowetting-on-dielectric *J. Appl. Phys.* **92** 4080–7
[15] Kipphan H (ed) 2001 *Handbook of Print Media: Technology and Production Methods* (Berlin: Springer)
[16] Young T 1805 An essay on the cohesion of fluids *Phil. Trans. R. Soc. Lond.* **95** 65–87
[17] Dupré A 1869 *Théorie Mécanique de la Chaleur* (Paris: Gauthier-Villars) pp 367–70

[18] Van Oss C J 2006 *Interfacial Forces in Aqueous Media Part I* (Boca Raton, FL: CRC press)
[19] Liston E M, Martinu L and Wertheimer M R 1993 Plasma surface modification of polymers for improved adhesion: a critical review *J. Adhes. Sci. Technol.* **7** 1091–27
[20] Yi U-C and Kim C-J 2006 Characterization of electrowetting actuation on addressable single-side coplanar electrodes *J. Micromech. Microeng.* **16** 2053–9
[21] Peregrine D H, Shoker G and Symon A 1990 The bifurcation of liquid bridges *J. Fluid. Mech.* **212** 25–39